Proceedings of the ASME 2021
International Mechanical Engineering Congress and Exposition
IMECE2021
November 1-5, 2021, Virtual, Online

IMECE2021-70515



# HIGH STRAIN RATE IMPACT ON CARBON NANOSTRUCTURES USING MOLECULAR DYNAMICS SIMULATIONS

**Matheus Prates[1], Ian Durr[1], Jungkyu Park[1]*, Giovanny Espitia[1], and Braden Peterson[2]**

[1]Kennesaw State University Kennesaw, Kennesaw, GA, USA
[2]Wheeler High School, Marietta, GA

*Corresponding author: jpark186@kennesaw.edu

## ABSTRACT

*In the present study, we researched the behavior of graphene experiencing high strain rate impacts by employing molecular dynamics simulations. Graphene with various thicknesses are selected for the study. A silver particle is designed to impact these carbon nanostructures with pre-specified speeds. The amount of energy absorbed during impacting graphene is calculated from the change in the kinetic energy of the silver particle before and after the impact. Graphene is shown to have excellent flexibility and its structural integrity is retained under a high strain rate impact. At an impact velocity of 4 km/s, a single layer of graphene absorbed 6.5 keV without any damage in the structure. The impact energy used to fracture graphene is shown to increase linearly with an increase in the thickness of graphene; the absorbed energy during breaking seven layers of graphene was 23 keV when the impact velocity was 10 km/s. It was also found that temperature does not affect the impact energy required to break a graphene sheet. The results obtained in the present research study will be used to accelerate the development of futuristic strong light-weight materials for military applications.*

Keywords: Graphene, Fracture, Molecular Dynamics

## 1. INTRODUCTION

Weight reduction is a prevalent requirement for any military weapons. Developing lightweight structural materials has been a priority research topic in many defense research agencies including the U.S. Department of Defense (DoD). Amongst lightweight materials proposed by researchers, carbon nanostructures such as graphene and carbon nanotube (CNT) are leading candidates due to the remarkable mechanical strength and exceptional transport properties of them as well as their porous architectures. Numerous practical applications in defense can be envisioned for carbon nanostructures. The lightweight, strong carbon nanostructures can be used as a body material for military vehicles, and this will improve their fuel efficiency and speed capability significantly. Also, since carbon nanostructures are thermally conductive, they can be used in a brake system of military vehicles, improving vehicles' braking performance and prolonging the brake's lifetime.

The extraordinary mechanical behavior of graphene has drawn attention from researchers since its first isolation in 2004 [1]. For example, Lee et al. [2] reported 130 GPa as the intrinsic strength of graphene and Jiang et al. [3] reported 1.1 TPa as its Young's modulus. To better utilize graphene in advanced electronics such as flexible electronics, it is critical to understand the fracture behavior of graphene under a dynamic loading. In this regard, Zhang et al. [4] used a nanoindentation to observe a brittle fracture and report a fracture toughness of 4MPa·$m^{1/2}$. They also used a molecular dynamics simulation and observed that a strain energy of 11.8 J/$m^2$ on the zigzag edge.

Hwangbo et al. [5] reported an even higher fracture toughness of 10.7 MPa·$m^{1/2}$; they found that cracks initiated at the grain boundaries of graphene are arrested by islands and wrinkles, slowing down the fracturing process that results in a higher fracture toughness that the theoretical predictions. Dewapriya et al. [6] used a molecular dynamics simulation to report that the strength of graphene is inversely proportional to the square root of the crack length. They found that quantized fracture mechanics is more useful in predicting crack propagation in graphene than Griffith's criterion. They also showed that the stress intensity factor of graphene decreases with an increase in temperature. Grantab et al. [7] studied graphene with tilt grant

boundaries using molecular dynamics and calculated the strength of graphene to be 125GPa. They revealed that as the grain-boundary angle increases, the fracture strength and strain at failure also increase. Jhon et al. [8] determined the orientation dependence of graphene fracture by using molecular dynamics; once the angle between the armchair direction and the direction of the tensile loading overcomes 12°, the strain increases exponentially with an increase in the angle, resulting in a large drop in the tensile strength. The study also showed that graphene exhibits quasi-isotropic elastic behavior, despite its anisotropic fracture response. Wang et al. [9] studied the effect of point defects on the fracture of graphene; Stone-Wales (SW) defects decrease the fracture strength of graphene by 21.7% for a S-$W_1$ defect or 45.3% for a S-$W_2$ defect. For a sheet with a 3-vacancy defect, the drop in the fracture strength is 37.3% for 300k, 40.2% for 500k, and 42.4% for 900k. Lee et al. [10] used a microscopic silica sphere fired at speeds 3,000 $s^{-1}$ at a graphene sheet with a thickness of 10 ~ 100 nm. The velocity of the particle before and after penetration was used to estimate the energy lost during the impact. They reported that the impact creates three to six cracks, propagated outward, forming a petal shape. The penetration energy was found to be 0.030 times the thickness of the impact area for a projectile speed of 900m/s. This corresponds to 1.26MJ/kg.

In the present research study, we aim to understand the fracture mechanism of graphene by using molecular dynamics simulations. A silver nanoparticle is forced to impact graphene with different number of layers. Impact energy absorbed by the graphene sheets during impact is then estimated.

## 2. SIMULATION METHOD

Molecular dynamics simulations are used to investigate the mechanical behavior of graphene during high-speed impact. The Large-scale Atomic/Molecular Massively Parallel simulator (LAMMPS) [11] is employed throughout the simulations in this study. A single layer of graphene simulated in the present research study is comprised of 96, 288 carbon atoms providing an area of 19,420 $Å^2$. To simulate the projectile, silver was chosen. The projectile is comprised of 864 atoms arranged in an FCC structure with a lattice parameter of 4.09 Å [12] (Figure 1).

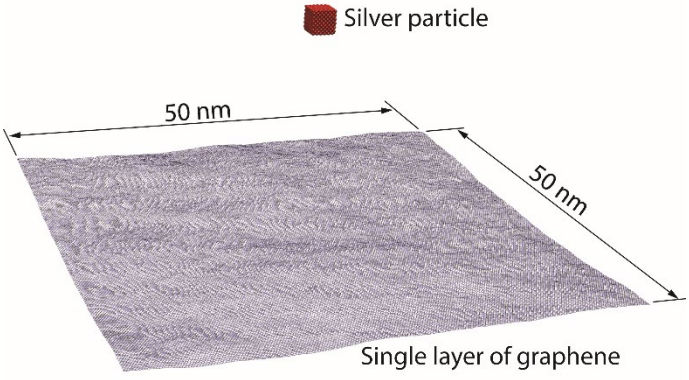


**FIGURE 1**: Graphene sheet and silver nanoparticle simulated in this research study.

The 2nd generation Reactive Empirical Bond Order (REBO) potential [13] that has been repeatedly used for carbon-based nanomaterials [14, 15] is used to describe the interaction between carbon atoms in graphene. The REBO potential allows for bonds to form and break with associated changes in hybridization within a classical potential. The REBO potential is described by the functional,

$$E_{REBO} = \sum_i \sum_{j>i} [V_r(r_{ij}) - B_{ij}^* V_a(r_{ij})] \quad (1)$$

where the term $r_{ij}$ corresponds to the distance between atoms $i$ and $j$. Here, the pair-additive interactions that described both interatomic repulsions and attractions are modeled by the terms $V_r(r_{ij})$ and $V_a(r_{ij})$. These terms are defined by,

$$V_r(r) = f_c(r)\left(1 + \frac{Q}{r}\right) A e^{(-\alpha r)} \quad (2)$$

$$V_a(r) = f_c(r) \sum_{n=1}^{3} B_n e^{(-\beta_n r)} \quad (3)$$

respectively. Here, $Q$, $A$, α, $B_n$, and $\beta_n$ represent constants and the pair-wise function $f_c(r)$, describe the cutoff function represented by,

$$f_c = \begin{cases} 1, r < R_{min} \\ \frac{\left\{1+\cos\left(\frac{\pi(r-R_{min})}{R_{max}-R_{min}}\right)\right\}}{2}, R_{min} < r < R_{max} \\ 0, r > R_{max} \end{cases} \quad (4)$$

where the upper and lower limits $R_{max}$ and $R_{min}$ equal 1.7 Å and 2.0 Å, respectively. In the present study, the values of constants correspond to those set by Brenner [13]. The usage of this potential to properly study the fracture of graphene has been demonstrated by Zhang [16], where the REBO potential was used to examine various forms of fracture including mode I toughness, dynamic, and impact. To define the interactions between Ag atoms, the Embedded – Atom Model (EAM) potential first proposed by Daw *et al.* [17] was used. The EAM potential has been purposefully optimized for systems with no directional bonding, thus being limited to only metals and its alloys. This potential has been proven to be compatible with Ag by Rassoulinejad-Mousavi [18], where the usage of EAM enabled the study of both tensile and shear strain of various metals at the nano-scale, including the one present in this study. EAM defined by the functional,

$$E_{tot} = F_\alpha\left(\sum_{i \neq j} \rho_\beta(R_{ij})\right) + \frac{1}{2}\sum_{i \neq j} \varphi_{ij}(R_{ij}) \quad (4)$$

Where $F_\alpha$ is a function of the atomic electron density corresponding to the embedding energy between the $i^{th}$ and $j^{th}$ atom. The term $F_\alpha$ is universal regarding the source of electron density. The terms $\rho_\beta(R_{ij})$, $\varphi_{ij}(R_{ij})$ correspond to the pair potential interaction between the atoms $i$ and $j$. Where, the expression $\rho_\beta(R_{ij})$ is the same as the total sum of atoms $j$ that do not equal $i$ in the function $\rho_j^a(R)$ which represents the

electron density contributed by the atom $j$ and the expression $\varphi_{ij}(R_{ij})$ corresponds to the pair repulsion between the atoms $i$ and $j$ separated by a distance $R_{ij}$. Here, the required parameters including density and charge are defined by the metal unit in LAMMPS. Since our simulation consisted of more than one type of atom, a third potential is necessary to properly define the C – Ag interactions. For this reason, the Lennard Jones (LJ) [19, 20] potential was used. This potential is of type pair as opposed to multi body, thus increasing efficiency in terms of run-time and associated costs. The LJ potential is described by the function,

$$V_{LJ} = 4\varepsilon[(\frac{\sigma}{r})^{12} - (\frac{\sigma}{r})^{6}] \quad (5)$$

Where the term $r$ is the distance between two interacting particles, $\varepsilon$ corresponds to the dispersion energy, and $\sigma$ represents the distance at which the potential energy $V$ equals zero. Note, that the minimum distance for $r$ is $2^{1/6}\sigma$. In the present study, the values of $\varepsilon$ and $\sigma$ are .031 and 2.3 respectively. These values were selected based on the work done by Das et al. [17]. In order to run the simulation, a hybrid pair coefficient must be introduced in the source code as to enable the listed potentials or pair styles to work in conjunction. This hybrid works by assigning a unique potential to an arbitrary pair of atoms. In this study, different impact velocities that range from 10 to 100 Å/ps (picosecond) are tested at different temperatures (200K, 300K, 400K, 600K). The impact energy is calculated from the difference in the kinetic energies of a silver particle before and after the impact.

## 3. RESULTS AND DISCUSSION

Figure 2a shows the change in kinetic energy of a silver particle during impacting a single layer of graphene. The kinetic energy change is increased with an increase in impact velocity until the graphene is fractured. There is no noticeable change in the amount of kinetic energy once the velocity reaches high enough to penetrate through the graphene sheet. It is interesting to note that the highest energy absorbed without fracturing graphene is higher than the impact energy absorbed when the graphene was fractured; the absorption energy was 6 keV at the impact velocity of 4 km/s while the absorption energy became 4.5 keV when the impact velocity of a silver particle was increased to 5 km/s, fracturing graphene. This is another indicator of the high flexibility of graphene. Figure 3 illustrates the evolution of the fracture of graphene during impacting a silver nanoparticle. It is shown that a large shock wave is generated as soon as the silver particle impacts the graphene sheet (Figure 3b). It should be noted that the propagation of the shock wave is limited by the simulation box size. However, the large size of graphene we simulated in this research prevents the reflection of the shock wave before the completion of fracture. Although periodic boundary condition is imposed, the wavelength of atomic vibrations cannot exceed the size of the simulation box. Therefore, we expect that the maximum impact energy absorbed before fracture will become larger as we increase the size of graphene. We will provide the effect of graphene size on the kinetic energy change during impact in another research study in the near future.

Figure 2b shows the change in the kinetic energy of a silver nanoparticle during impacting a single layer of graphene at different temperatures. Temperature does not seem to affect the impact energy. When the impact velocity is 5 km/s, however, the kinetic energy change becomes abnormally high at 400K. To understand this better, the deformed graphene sheets at 300K and 400K are drawn in Figure 4. The size of the deformed region in graphene at 400K is much larger when compared to the size of the deformed region in the graphene at 300K. This shows that more energy is consumed to deform graphene at 400K. However, it is not clear why graphene at 400K shows a higher flexibility when compared to graphene sheets at different temperatures.

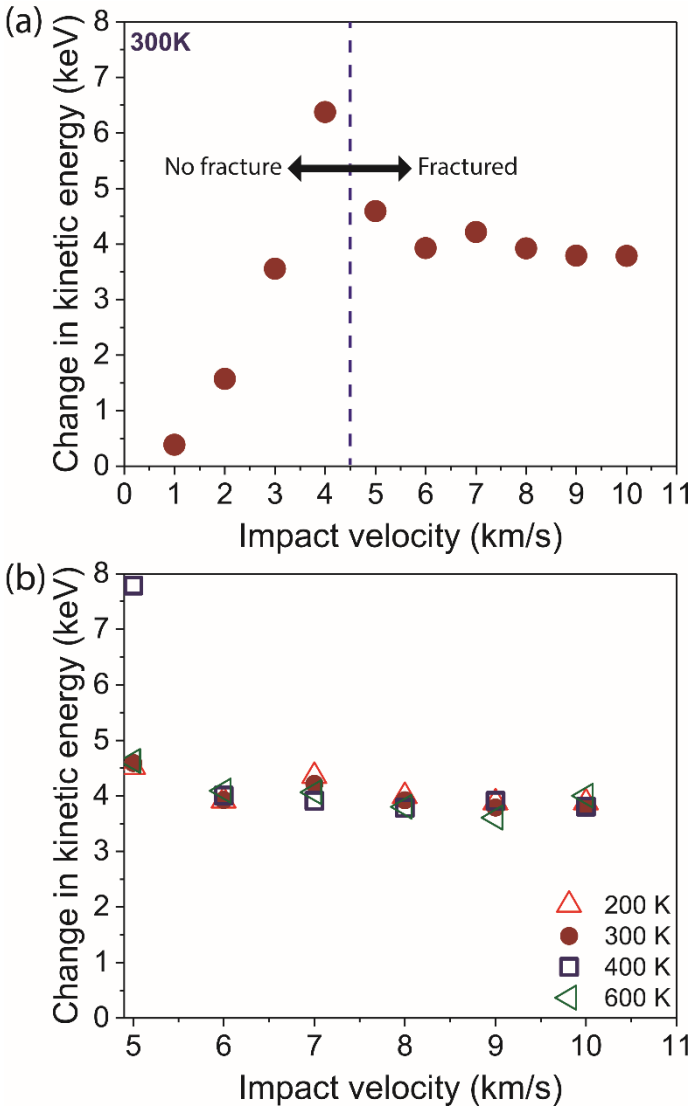


**FIGURE 2**: (a) change in kinetic energy of a silver particle during impacting a single layer of graphene. (a) change in kinetic energy during impacting a graphene sheet at different temperatures.

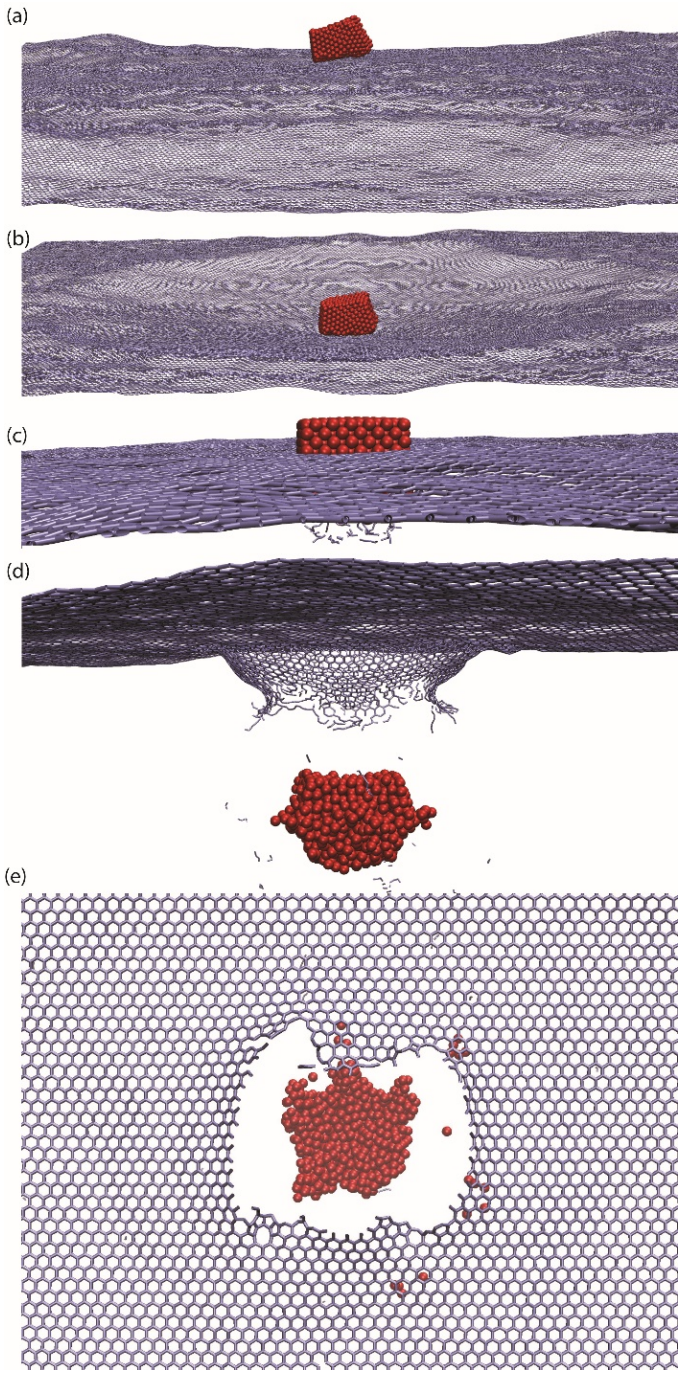


**FIGURE 3**: The evolution of the fracture of a graphene sheet during impact.

Xia et al. [21] also used a monolayer graphene sheet and a high velocity projectile to impact that graphene sheet. They used a sheet of similar size used in our research at 50 x 50 $nm^2$ with a projectile radius of 25Å and a velocity of 2km/s. This research was conducted to study the total amount of energy lost from the projectile after the impact; the result from this research is very similar to our results at similar speeds. At speeds of 2 km/s the projectile experienced a change of energy of roughly 2118 eV, which is close to our result of just under 5000 eV at 5 km/s at just over double the velocity. This research has also experienced the phenomenon of the projectile bouncing back at 2 km/s when the projectile radius was reduced to 24Å, whereas our graphene sheet reflected the projectile back at a velocity of 4 km/s or below. This shows that the size of the projectile will certainly have an effect on how the graphene handles the impact energy in future experiments.

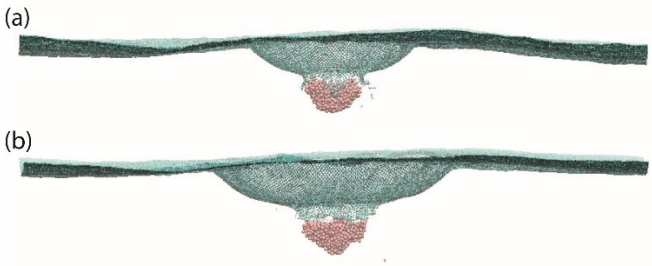


**FIGURE 4**: (a) Deformation of graphene at 300K with the impact velocity of 5 km/s. (b) Deformation of graphene at 400K with the impact velocity of 5 km/s.

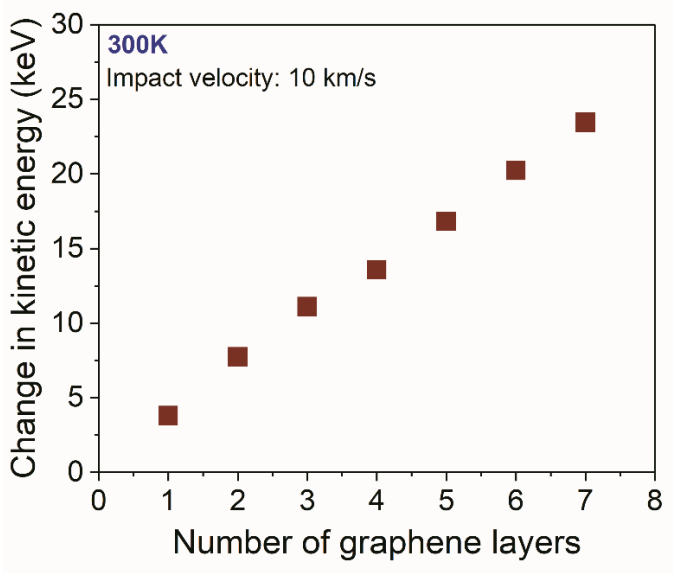


**FIGURE 5**: Change in kinetic energy during impacting graphene with different number of layers.

Fracture of graphene with different number of layers is studied using the same simulation method at an impact velocity of 10 km/s (Figure 5). The results show that the kinetic energy change is increased almost linearly with an increase in the number of graphene layers. This indicates that the amount of energy that is required to break each layer is the same regardless of the location of the graphene layer. Figure 6 illustrates the fracture graphene with multiple layers. The shape of the fracture surface in multiple layers of graphene (Figure 6b) is more circular than that in single layer of graphene (Figure 3d). Also, the silver nanoparticle is damaged more as the number of layers of graphene is increased. In this regard, Hwangbo et al. [5], also

showed that larger graphene thickness hinders a crack propagation under stresses. Xiao et al. [21] also noted that multi-layer graphene results can experience more efficient impact protection, which reinforces our results of when an increased number of graphene sheets increased the change in kinetic energy at 300K with the projectile velocity of 10 km/s.

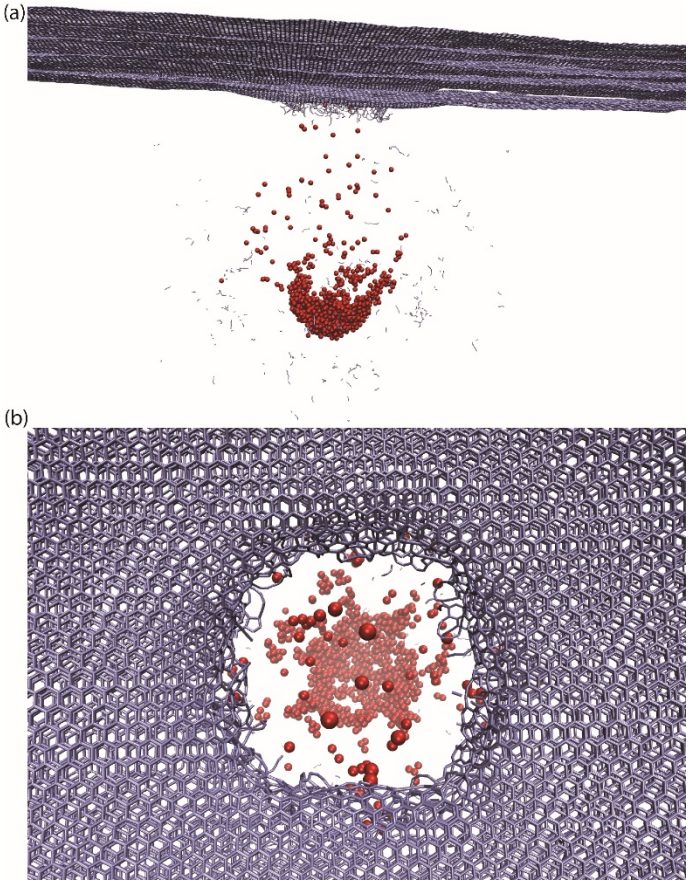


**FIGURE 6**: Illustration of the fracture of multiple layers of graphene.

Griffith's Theory is often used to understand and measure the material's resistance to cracking when cracks begin to form on the surface of the material. It is also utilized to understand a specimen's fracture toughness. Researchers [4, 22] reported that this theory can be applied to graphene as well. Graphene that we have simulated experienced defects due to the strain upon the impact of the silver material. That defect will allow the graphene to resist crack propagation. Research conducted by Zhang et al. [22] tested one-atom thick graphene material and obtained the fracture toughness of the material by using Griffith's Theory. The graphene demonstrated an exceptionally high fracture toughness of 6.1±0.6 MPa and the increase of fracture toughness was the result of the defects that were experienced on the specimen. The defects allowed an increase in the opening at the tip of the fracture and facilitated the stress relaxation and the energy release. This reinforces the results previously mentioned when graphene at 400K has a higher change in energy at an impact of 5 km/s compared to 300K. This could possibly be due to the fact that the larger deformed area absorbs more of the energy. An increase in layer count has also resulted in higher change in kinetic energy due to the improved facilitation of the impact energy and resistance to fractures due to the defects. However, it is questionable whether Griffith' theory can be applied to a material that undergoes a high-speed impact.

Figure 7 shows the change in kinetic energy during the impact on graphene with seven layers. A substantial difference is identified when Figure 7 is compared to Figure 2a. Unlike single layer of graphene, the kinetic energy is shown to increase with an increase in the impact velocity. In this regard, researchers [16, 21] agree that the specific penetration energy of graphene increases as velocity increases. Lee et al. [23] also found that as velocity increases, the penetration energy relative to the thickness of the impact area increases. In addition, Dewapriya and Miller [24] measured the impact pressure of silicon carbide as 12.9GPa for 650m/s and 17GPa for 800m/s. The common pattern in this data set is that all of the properties directly related to velocity increase, which implies that velocity increases as well.

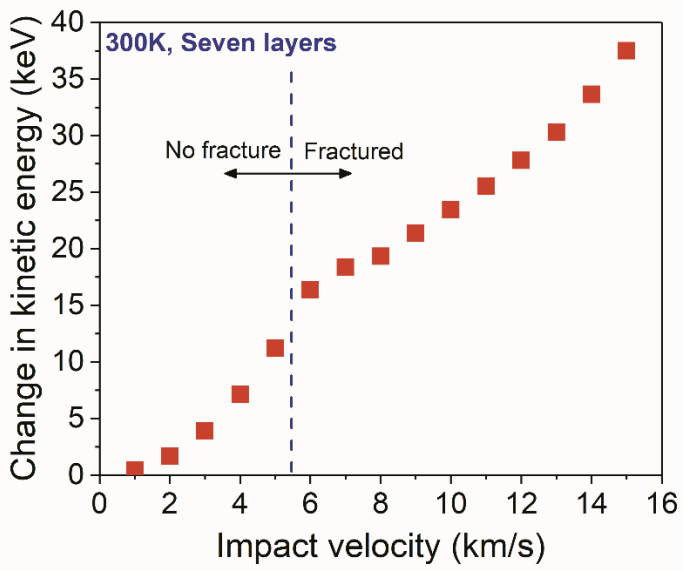


**FIGURE 7**: Change in kinetic energy during the impact on seven layers of graphene.

As explored in this study, a monolayer of graphene is capable of stopping nano projectiles traveling at approximately 4.5 km/s. This, along with its other notable mechanical properties, demonstrate the potential graphene has in the defense industry. Currently, the material of choice for bulletproof vests and other armored equipment is Kevlar®, which was developed by DuPont. The latter is a synthetic fiber with formula [-CO-$C_6H_4$-CO-NH-$C_6H_4$-NH-]$_n$ that counts with high mechanical and thermal properties [25]. One example being a tensile strength of 3,620 MPa [26], which is theoretically five times stronger than steel. However, for this fiber to be effective in the demands of

modern warfare, it must be stacked in several layers, which not only increases weight, but also limits mobility if employed for protective equipment. By using the results obtained by Khodadadi et al. [27], one is able to examine the energy absorption of two layers of Kevlar® and contrast it with Figure 2a. In their study, the projectile had a diameter of 10mm and a mass of 9.32 Kg. As one can denote, a single layer of graphene is capable of absorbing enough energy to stop the projectile traveling at 4.5 km/s, whereas the bilayer of Kevlar® was able to stop projectiles traveling at a maximum speed of approximately 116 m/s. Please note that while our results were obtained through computational methods, the study mentioned obtained the results through physical experimentation. Interestingly, as the accessibility for graphene increases, the opportunity for a more direct comparison becomes feasible and open for further study. This short comparison is simply another indicator of the potential graphene can have for military and tactile applications. The scalable production of graphene has been a difficult challenge throughout this field of research especially without compromising the materials strength capabilities. Karim et al. [28] studied a scalable method to produce graphene through chemical reduction of graphene oxidation to introduce a stable way to create wearable textiles. The process involved running the fabric through a pad-dry unit with reduced graphene oxide to coat the material. From their study, they were successful by using the chemical, Na2S2O4, as a reducing agent and used at a relatively lower temperature of 100 °C in the process. The reducing agent, Na2S2O4, and shows a promising result in increase of carbon content and an increase of C-O ratio. This increase in carbon ratio, proved to have a significant increase in tensile strength in graphene oxide treated fabrics by 20% to 30% and an enhancement in flexibility. According to Karim et al. [28], tensile strength and flexibility would increase even higher with additional padding passes through reduced graphene oxide. This process is just an example of how scalable production of graphene can be similar to textile productions that normally wouldn't use graphene as the core material, and it shows to be a potential solution for producing future military material.

## CONCLUSIONS

In the present research study, we employed molecular dynamics simulations to investigate the mechanical behavior of graphene with different thicknesses under high strain rate impact. The highest energy absorbed in a single layer of graphene without fracture was 6.5 keV at an impact velocity of 4 km/s. Once the impact velocity becomes high enough to fracture graphene, the amount of energy used to break graphene does not change with an increase in the impact velocity. The impact energy absorbed during the fracture of graphene increases linearly with an increase in the thickness of graphene. The results obtained in this research will be used to develop light weight strong future materials that can be used in military applications.

## ACKNOWLEDGEMENTS

This work made use of the High Performance Computing resource at Kennesaw State University. The authors would like to acknowledge NESEL (Nuclear Energy, Science, and Engineering Laboratory) at Kennesaw State University for supporting this research study.

## REFERENCES

[1] K. S. Novoselov *et al.*, "Electric field effect in atomically thin carbon films," *science,* vol. 306, no. 5696, pp. 666-669, 2004.

[2] C. Lee, X. Wei, J. W. Kysar, and J. Hone, "Measurement of the elastic properties and intrinsic strength of monolayer graphene," *science,* vol. 321, no. 5887, pp. 385-388, 2008.

[3] J.-W. Jiang, J.-S. Wang, and B. Li, "Young's modulus of graphene: a molecular dynamics study," *Physical Review B,* vol. 80, no. 11, p. 113405, 2009.

[4] P. Zhang *et al.*, "Fracture toughness of graphene," *Nature communications,* vol. 5, no. 1, pp. 1-7, 2014.

[5] Y. Hwangbo *et al.*, "Fracture characteristics of monolayer CVD-graphene," *Scientific reports,* vol. 4, no. 1, pp. 1-9, 2014.

[6] M. Dewapriya, R. Rajapakse, and A. Phani, "Atomistic and continuum modelling of temperature-dependent fracture of graphene," *International Journal of Fracture,* vol. 187, no. 2, pp. 199-212, 2014.

[7] R. Grantab, V. B. Shenoy, and R. S. Ruoff, "Anomalous strength characteristics of tilt grain boundaries in graphene," *Science,* vol. 330, no. 6006, pp. 946-948, 2010.

[8] Y. I. Jhon, Y. M. Jhon, G. Y. Yeom, and M. S. Jhon, "Orientation dependence of the fracture behavior of graphene," *Carbon,* vol. 66, pp. 619-628, 2014.

[9] M. Wang, C. Yan, L. Ma, N. Hu, and M. Chen, "Effect of defects on fracture strength of graphene sheets," *Computational Materials Science,* vol. 54, pp. 236-239, 2012.

[10] J.-H. Lee *et al.*, "Wafer-scale growth of single-crystal monolayer graphene on reusable hydrogen-terminated germanium," *Science,* vol. 344, no. 6181, pp. 286-289, 2014.

[11] S. Plimpton, "Fast parallel algorithms for short-range molecular dynamics," *Journal of computational physics,* vol. 117, no. 1, pp. 1-19, 1995.

[12] W. P. Davey, "Precision measurements of the lattice constants of twelve common metals," *Physical Review,* vol. 25, no. 6, p. 753, 1925.

[13] D. W. Brenner, O. A. Shenderova, J. A. Harrison, S. J. Stuart, B. Ni, and S. B. Sinnott, "A second-generation reactive empirical bond order (REBO) potential energy expression for hydrocarbons," *Journal of Physics: Condensed Matter,* vol. 14, no. 4, p. 783, 2002.

[14] S. Okamoto and A. Ito, "Mechanical Properties of Single Crystal Diamond Estimated by Molecular Dynamics Simulation with the Second-Generation REBO Potential," *MRS Online Proceedings Library (OPL),* vol. 1362, 2011.

[15] A. Shakouri, T. Ng, and R. Lin, "A new REBO potential based atomistic structural model for graphene sheets," *Nanotechnology,* vol. 22, no. 29, p. 295711, 2011.
[16] T. Zhang, X. Li, and H. Gao, "Fracture of graphene: a review," *International Journal of Fracture,* vol. 196, no. 1-2, pp. 1-31, 2015.
[17] S. R. Das *et al.*, "Single-layer graphene as a barrier layer for intense UV laser-induced damages for silver nanowire network," *ACS nano,* vol. 9, no. 11, pp. 11121-11133, 2015.
[18] S. M. Rassoulinejad-Mousavi and Y. Zhang, "Interatomic potentials transferability for molecular simulations: A comparative study for platinum, gold and silver," *Scientific reports,* vol. 8, no. 1, pp. 1-10, 2018.
[19] J. E. Jones, "On the determination of molecular fields.—I. From the variation of the viscosity of a gas with temperature," *Proceedings of the Royal Society of London. Series A, Containing Papers of a Mathematical and Physical Character,* vol. 106, no. 738, pp. 441-462, 1924.
[20] J. E. Jones, "On the determination of molecular fields.—II. From the equation of state of a gas," *Proceedings of the Royal Society of London. Series A, Containing Papers of a Mathematical and Physical Character,* vol. 106, no. 738, pp. 463-477, 1924.
[21] K. Xia, H. Zhan, D. a. Hu, and Y. Gu, "Failure mechanism of monolayer graphene under hypervelocity impact of spherical projectile," *Scientific reports,* vol. 6, no. 1, pp. 1-10, 2016.
[22] Z. Zhang *et al.*, "Crack Propagation and Fracture Toughness of Graphene Probed by Raman Spectroscopy," *ACS nano,* vol. 13, no. 9, pp. 10327-10332, 2019.
[23] J.-H. Lee, P. E. Loya, J. Lou, and E. L. Thomas, "Dynamic mechanical behavior of multilayer graphene via supersonic projectile penetration," *Science,* vol. 346, no. 6213, pp. 1092-1096, 2014.
[24] M. Dewapriya and R. Miller, "Molecular dynamics study of the penetration resistance of multilayer polymer/ceramic nanocomposites under supersonic projectile impacts," *Extreme Mechanics Letters,* vol. 44, p. 101238, 2021.
[25] V. Radić, "Kevlar and ballistic protection," *Vojnotehnički glasnik,* vol. 44, no. 1, pp. 79-87, 1996.
[26] J. Quintanilla, "Microstructure and properties of random heterogeneous materials: a review of theoretical results," *Polymer Engineering & Science,* vol. 39, no. 3, pp. 559-585, 1999.
[27] A. Khodadadi *et al.*, "High velocity impact behavior of Kevlar/rubber and Kevlar/epoxy composites: A comparative study," *Composite Structures,* vol. 216, pp. 159-167, 2019.
[28] Karim et al., “Scalable Production of Graphene-Based Wearable E-Textiles” ACS Nano 2017, 11, 12266-12275